

Neutral Pion Photoproduction in a Regge Model

V. Mathieu*

*Center for Exploration of Energy and Matter, Indiana University, Bloomington, IN 47403 and
Physics Department, Indiana University, Bloomington, IN 47405*

G. Fox

School of Informatics and Computing, Indiana University, Bloomington, IN 47405, USA

A. P. Szczepaniak

*Center for Exploration of Energy and Matter, Indiana University, Bloomington, IN 47403
Physics Department, Indiana University, Bloomington, IN 47405 and*

Thomas Jefferson National Accelerator Facility, Newport News, VA 23606, USA

(Dated: March 4, 2022)

The reaction $\gamma p \rightarrow \pi^0 p$ is investigated in the energy range above the resonance region. The amplitudes include the leading Regge singularities in the cross-channel and correctly describe the differential cross section for beam energies above 4 GeV and for the s -channel scattering angle $\cos\theta_s \geq 0.6$. The energy dependence of the beam asymmetry and the reaction $\gamma n \rightarrow \pi^0 n$ seem to be quantitatively consistent with the Regge-pole dominance.

PACS numbers: 13.75.Gx, 13.85.Fb, 11.55.Jy, 12.40.Nn

I. INTRODUCTION

Single pion photoproduction on a nucleon is one of the key reactions in hadron physics. At low energies, it is used to excite nucleon resonances while at high energies it can be used to test predictions of Regge theory, *e.g.* factorization of Regge poles [1]. The two regimes are analytically connected and relations *e.g.* finite energy sum rules (FESR), can be derived to constrain resonance parameters by the cross-channel Reggeons [2]. In recent years the CLAS experiment at JLab collected data on single pion production using photon beams with energies ranging from $E_\gamma = 1.275$ GeV to 5.425 GeV [3]. This energy range overlaps with both, the resonance and the Regge regions. Once the data is analyzed it will open the possibility to perform finite energy sum rules studies of pion photoproduction based on data from a single experiment. This will reduce systematic uncertainties and possibly help to clarify some of the outstanding theoretical issues encountered in earlier studies [4]. Single pion photoproduction will also be among the first reactions studied with the newly completed GlueX detector that will use highest energy photons from the recently upgraded CEBAF accelerator.

There are several neutral pion photoproduction models developed to describe the nucleon resonance region [5–8], which is not the case of the high-energy regime. Regge description has not been updated in the recent past, with the exception of Ref. [9]. In view of the forthcoming measurements it is therefore necessary to revisit the theoretical models. This is the main focus of this paper. According to Regge theory, at asymptotically large center

of mass energies reaction amplitudes are determined by the right-most singularity in the complex angular momentum plane of the cross-channel partial waves. Except for elastic scattering, which is dominated by the Pomeron, these are the Regge poles. A single Regge pole contribution factorizes into a product of “couplings/residues” and “propagators”. This property enables classification of Regge poles similar to that of elementary particles [10]. As the center of mass energy decreases, sub-leading angular momentum plane singularities become relevant including Regge poles with lower intercept *aka.* daughter trajectories and Regge cuts. Since the ultimate goal is to connect the Regge and resonance regions and make predictions for the energy range of the CLAS measurement, in this paper we also explore these sub-leading contributions. We focus on scattering in the forward direction where the dominant Regge singularities originate from the t -channel exchanges. The goal is to find a simple, albeit consistent with Regge theory, parametrization that once the CLAS data is analyzed, can be applied in a simultaneous study of the resonance and Regge regions *e.g.* using finite energy sum rules.

The paper is organized as follows. In Section II we discuss the t -channel amplitudes and their connection to the direct, s -channel observables. Conventions and details of calculations are given in Appendix A and B. Specification of the Regge exchange model is given in Section III. Analysis of existing data is summarized in Section IV and predictions for the CLAS energy range and for $E_\gamma = 9$ GeV, relevant for the upcoming experiments at JLab are given in Section V. Conclusions are summarized in Section VI.

* mathieu@indiana.edu

II. FORMALISM

The reaction $\gamma(k, \lambda)N(p_2) \rightarrow \pi(q)N(p_4)$ describing pion with momentum q , the photon with momentum k and helicity λ , and a pair of nucleons with momenta p_2 and p_4 is given in terms of four invariant amplitudes, which are linearly related to four helicity amplitudes. The scalar amplitudes are functions of two independent Mandelstam variables, $s = (k + p_2)^2$ and $t = (k - q)^2$. The helicity amplitudes are frame dependent. The two relevant frames for our discussion are the s -channel and t -channel frames. They correspond to the center of mass frame of the reaction $\gamma N \rightarrow \pi^0 N$ for the s -channel and $\gamma \pi^0 \rightarrow \bar{N}N$ for the t -channel, respectively. Helicity amplitudes in the s -channel are used to compute observables. At high energies and small scattering angles the s -channel amplitudes are dominated by singularities in the complex angular plane of the t -channel. Helicity amplitudes in the t -channel are therefore needed to identify the allowed Regge exchanges. Detailed analysis of the t -channel helicity amplitudes and their quantum numbers is given in Appendix A. The s -channel helicity amplitudes and the observables are discussed in Appendix B. In this section we summarize the main results.

The invariant amplitudes, $A_i(s, t)$ multiply four independent tensors constructed from the photon polarization vector, two Dirac spinors and particle momenta constrained to fulfill global symmetry requirements and gauge invariance. The tensors are conventionally chosen from the Chew-Goldberger-Low-Nambu (CGLN) basis [11], and the helicity amplitudes are given by

$$A_{\mu_4, \mu_2 \mu_1}^s(s, t) = \bar{u}_{\mu_4}(p_4) \sum_{i=1}^4 A_i(s, t) M_i u_{\mu_2}(p_2), \quad (1a)$$

$$A_{\lambda_4 \lambda_2, \lambda_1}^t(s, t) = \bar{u}_{\lambda_4}(p_4) \sum_{i=1}^4 A_i(s, t) M_i v_{\lambda_2}(-p_2), \quad (1b)$$

with the subscripts s and t referring to the s and t channels, and in the following we use μ_i and λ_i to denote particle helicities in the two channels. The tensors M_i are given in (A2). The scalar functions A_i have dynamical singularities in s and t while the helicity amplitudes have additional singularities arising from the kinematical factors in Eq. (1). To identify t -channel reggeons it is necessary to identify t -channel helicity amplitudes free from kinematical singularities. Kinematical singularities are related to presence of spin and can be related to singularities of the Wigner- d functions. The rotational functions can be written as $d_{\lambda' \lambda}^J(z_t) = \xi_{\lambda' \lambda}(z_t) P_{\lambda' \lambda}^J(z_t)$ where P^J is a polynomial and

$$\xi_{\lambda' \lambda}(z_t) = \left(\frac{1 - z_t}{2} \right)^{\frac{1}{2}|\lambda' - \lambda|} \left(\frac{1 + z_t}{2} \right)^{\frac{1}{2}|\lambda' + \lambda|}, \quad (2)$$

with $\lambda = \lambda_1 - \lambda_3 = \lambda_1$, $\lambda' = \lambda_2 - \lambda_4$. As shown in Appendix A singularities in s of the t -channel helicity amplitudes can be removed by dividing helicity amplitudes

by ξ ,

$$\hat{T}_{\lambda' \lambda} = \xi_{\lambda' \lambda}^{-1}(z_t) A_{\lambda_4 \lambda_2, \lambda_1}^t(s, t). \quad (3)$$

The remaining singularities of \hat{T} in s are dynamical in nature. Since Reggeons have well defined quantum numbers in the t -channel, they will contribute to specific linear combination of the invariant amplitudes A_i . Helicity amplitudes are not eigenstates of parity and the t -channel parity conserving helicity amplitudes (PCHAs) correspond to linear combination, [12, 13]

$$\hat{T}_{\lambda' \lambda}^\eta = \frac{1}{\sqrt{2}} \left(\hat{T}_{\lambda' \lambda} + \eta(-1)^{\lambda'} \hat{T}_{\lambda' - \lambda} \right). \quad (4)$$

where η is the t -channel naturality, *i.e.* $\eta = P(-)^J$ where P is the intrinsic parity and J is the spin of the exchange Reggeon in the t -channel. As shown in the Appendix A, the relations between PCHAs and invariant amplitudes are [14]

$$\hat{T}_{01}^+ = -2k_t \sqrt{t} (-A_1 + 2MA_4) \quad (5a)$$

$$\hat{T}_{01}^- = -4p_t k_t (A_1 + tA_2) \quad (5b)$$

$$\hat{T}_{11}^+ = -2k_t (2MA_1 - tA_4) \quad (5c)$$

$$\hat{T}_{11}^- = 4p_t k_t \sqrt{t} A_3 \quad (5d)$$

with M being the nucleon mass. The photon momentum, k_t and the proton momentum p_t evaluated in the t -channel *cf.* Eq. (A4), contain the remaining kinematical singularities in t . We can now define four amplitudes, free of kinematical singularities that have well defined quantum numbers (η and CP) in the t -channel. These are,

$$F_1 = -A_1 + 2MA_4, \quad \eta = +1, \quad CP = +1, \quad (6a)$$

$$F_2 = A_1 + tA_2, \quad \eta = -1, \quad CP = -1, \quad (6b)$$

$$F_3 = 2MA_1 - tA_4, \quad \eta = +1, \quad CP = +1, \quad (6c)$$

$$F_4 = A_3, \quad \eta = -1, \quad CP = +1. \quad (6d)$$

Only negative charge conjugation, $C = -1$ exchanges, couple to $\gamma\pi^0$. For positive naturality, these correspond to vector trajectories ω ($I^G = 0^-$) and ρ ($I^G = 1^+$) and contribute to F_1 and F_3 . For negative η the axial-vector trajectories h ($I^G = 0^-$) and b ($I^G = 1^+$) contribute to F_2 . There are no known mesons contributing to F_4 . The lowest mesons in the t -channel contributing to F_4 would be the ρ_2 and ω_2 with $J^{PC} = 2^{--}$. Therefore in the following we ignore the F_4 (although there are some indications that F_4 might not be exactly zero [15]).

Using the invariant amplitudes F_i defined in Eq. (6) one can compute all observables. In particular we are interested in the differential cross section and the single polarization asymmetries. The beam asymmetry is $\Sigma = (d\sigma_\perp - d\sigma_\parallel)/(d\sigma_\perp + d\sigma_\parallel)$ where $d\sigma_\perp$ ($d\sigma_\parallel$) is the differential cross section with photon polarization along the x (y) axis and the z axis along the direction of the photon momentum and y perpendicular to the reaction plane. The target (recoil) asymmetry is defined

as $T(R) = (d\sigma_{\uparrow} - d\sigma_{\downarrow})/(d\sigma_{\uparrow} + d\sigma_{\downarrow})$ and measures the asymmetry of the spin polarization of the target (recoil) nucleon.

At high energies, keeping only the leading s dependence in the kinematical factors relating the differential cross section to the scattering amplitude, one finds [15]¹

$$\frac{d\sigma}{dt} \approx \frac{1}{32\pi} \left[\frac{|F_3|^2 - t|F_1|^2}{4M^2 - t} + |F_2|^2 - t|F_4|^2 \right] \quad (7a)$$

$$\Sigma \frac{d\sigma}{dt} \approx \frac{1}{32\pi} \left[\frac{|F_3|^2 - t|F_1|^2}{4M^2 - t} - |F_2|^2 + t|F_4|^2 \right] \quad (7b)$$

$$T \frac{d\sigma}{dt} \approx \frac{1}{16\pi} \sqrt{-t} \operatorname{Im} \left[\frac{F_3 F_1^*}{4M^2 - t} + F_4 F_2^* \right] \quad (7c)$$

$$R \frac{d\sigma}{dt} \approx \frac{1}{16\pi} \sqrt{-t} \operatorname{Im} \left[\frac{F_3 F_1^*}{4M^2 - t} - F_4 F_2^* \right]. \quad (7d)$$

The differential cross section in physical units ($\mu\text{b GeV}^{-2}$) is obtained by multiplying the right hand sides by the conversion factor $1 = 389.4 \mu\text{b GeV}^2$. These asymptotic formulas are useful for identifying contributions from the individual Regge contributions to the amplitudes F_i . In numerical calculations that follow, for the differential cross section, we use the complete expression

$$\begin{aligned} \frac{d\sigma}{dt} = \frac{1}{64\pi} \frac{|k_t|^2}{4M^2 E_\gamma^2} \left[2|\sin \theta_t|^2 (|2p_t F_2|^2 - t|F_1|^2) \right. \\ \left. + (1 - \cos \theta_t)^2 |F_3 - 2\sqrt{t} p_t F_4|^2 \right. \\ \left. + (1 + \cos \theta_t)^2 |F_3 + 2\sqrt{t} p_t F_4|^2 \right], \quad (8) \end{aligned}$$

where E_γ is the beam energy in the laboratory frame. To check the validity of the asymptotic approximation, in Section V we compare the results obtained using Eq. (7) and Eq. (8). In calculations of the spin asymmetries, however, we use the asymptotic formulas of Eq. (7) since the finite- s corrections cancel in the ratio of cross sections.

Most of the available data comes from the proton target with only a few measurements of the differential cross sections on the neutron. The corresponding amplitudes are related by isospin symmetry. In the t -channel, the isospin decomposition for each of the four invariant amplitudes is given by [11]

$$A_{\alpha\beta}^a = A^{(+)} \delta^{a3} \delta_{\alpha\beta} + A^{(-)} \frac{1}{2} [\tau^a, \tau^3]_{\alpha\beta} + A^{(0)} \tau_{\alpha\beta}^a. \quad (9)$$

with $A^{(+)}$, $A^{(-)}$ and $A^{(0)}$ corresponding to t -channel isospin $I^G = 0^-, 1^-$ and 1^+ and a, α, β being the isospin indices for the pion, the two nucleons, respectively. Only

$A^{(+)}$ and $A^{(0)}$ contribute to π^0 photoproduction. We note that the isovector exchange contribution contributes with opposite sign to proton and neutron amplitudes, *i.e.*

$$A(\gamma p \rightarrow \pi^0 p) = A^{(+)} + A^{(0)}, \quad (10a)$$

$$A(\gamma n \rightarrow \pi^0 n) = A^{(+)} - A^{(0)}. \quad (10b)$$

III. THE REGGE MODEL

In this section we specify the model for the t -channel kinematical singularity free amplitudes $F_i(s, t)$. The contribution of a Regge pole, $R(s, t)$ and a Regge-Pomeron cut $R_c(s, t)$ to $F_i(s, t)$ have asymptotic energy dependence determined by the Regge trajectory $\alpha(t)$ [1, 12, 16]. The residues are analytical in t in the s -channel physical region and have zeros that are forced by spin considerations. In particular, in the physical region of the t -channel, net helicity in either, the $\gamma\pi^0$ or the $N\bar{N}$ vertex cannot exceed $J = \alpha(t)$ for non-negative, integer values of J . In addition, in the s -channel physical region the amplitude cannot have singularities other than threshold branch points. A simple model that builds in these constraints is given by,

$$R(s, t) = \frac{\pi}{\Gamma(\alpha(t))} \frac{1 - e^{-i\pi\alpha(t)}}{2 \sin \pi\alpha(t)} \left(\frac{s}{s_0} \right)^{\alpha(t)-1}, \quad (11)$$

$$R_c(s, t) = \frac{1}{\log(s/s_0)} \frac{\pi}{\Gamma(\alpha_c(t))} \frac{1 - e^{-i\pi\alpha_c(t)}}{2 \sin \pi\alpha_c(t)} \left(\frac{s}{s_0} \right)^{\alpha_c(t)-1}. \quad (12)$$

The energy dependence yields the expectation $s^2 d\sigma/dt \propto s^{2\alpha(t)}$ once the extra energy power coming from the half-angle factor in Eq. (2) is included. These expressions can in principle be multiplied by an analytical function of t , that can be, for example fixed by the data. To minimize the number of parameters in the model, we will attempt to fit the data with minimal such modifications (see below) observing that the scale s_0 already leads to an exponential fall off with t for $s > s_0 = 1 \text{ GeV}^2$ which is typical. For positive values of spin, $J = \alpha > 0$, the signature factor $1 - e^{-i\pi\alpha}$ is finite for the right exchanges, *i.e.* odd-spin mesons lying on the vector or axial-vector trajectories and it vanishes, canceling the zero of $\sin \pi\alpha$ for the wrong spin exchanges *i.e.* even-spin mesons. For negative odd-values of α there would be unphysical poles. The Γ function in the denominator is introduced to remove these poles from the s -channel physical region. It also leads to zeros of the amplitude at non-positive even integer values of α . As discussed above Eq. (11) $\alpha = 0$ is indeed forbidden by spin considerations since it is less than the magnitude of net helicity in the $\gamma\pi^0$ vertex. In principle there is no need for the amplitude to vanish at negative even-integer values of α . Thus the particular choice of using the Γ function to cancel the unphysical

¹ We corrected the sign of F_1 in the target and recoil asymmetries, *cf.* Appendix B.

poles of the so-called Regge propagator, $1/\sin \pi\alpha$, has to be confronted with the data and can in principle be modified if needed. We will further explore the consequences of this choice in Section IV and V.

For values of α which are not too far from positive integers Regge pole amplitudes are similar to this of particle exchange. We therefore use a one-particle-exchange model for a vector and axial-vector meson to impose further constraints. The t -channel amplitude for a vector meson exchange, *e.g.* $V = \rho, \omega$ is given by (*cf.* Appendix A)

$$\frac{i\varepsilon_{\alpha\beta\mu\nu}k^\mu\epsilon^\nu q^\alpha}{t-m_V^2}\bar{u}_4\left[g_4^V\gamma^\beta+g_1^V\gamma^{[\beta}\gamma^{\sigma]}(p_2-p_4)_\sigma\right]v_2 \\ =\bar{u}_4\left[\frac{g_4^VM_4+g_1^V(tM_1-M_2)}{t-m_V^2}\right]v_2, \quad (13)$$

where $\bar{u}_4 \equiv \bar{u}(p_4, \mu_4)$ and $v_2 \equiv v(-p_2, \mu_2)$ with the right hand side written in terms of the CGLN basis tensors M_i . Similarly for the axial vectors, $A = b, h$ one finds,

$$g_2^A\epsilon^\mu[k\cdot qg_{\mu\alpha}-q_\mu k_\alpha]\frac{\bar{u}_4\gamma_5 p^\alpha v_2}{t-m_A^2}=\frac{\bar{u}_4 g_2^A M_2 v_2}{t-m_A^2}. \quad (14)$$

Comparing with Eq. (1) one concludes that, for the vector contribution, $A_1 \propto g_1 t$, $A_2 \propto -g_1$ and $A_4 \propto g_4$. We also note that in the s -channel frame g_4 corresponds to helicity non-flip coupling and g_1 to helicity flip coupling. Near the pole, the tree-level propagator $1/(t-m_V^2)$, corresponds to $1/\sin \pi\alpha$. We also note that, as expected, the vector exchanges contribute only to F_1 and F_3 . Also, as expected we find that the axial vector change contributes only to F_2 via $A_2 \propto g_2^A$.

The data, as it will be described in the next section, indicate that corrections to the Regge pole approximation are needed. We then anticipate and add in our model the cut associated with the vector trajectory. Their role will be clarified by comparing to the data. The t -dependence of Regge-Pomeron cut residues is, *a priori*, different from that of the Regge poles. For simplicity, however, we will use the same t -dependence as for the corresponding pole. Taking these considerations into account leads to the following expressions for the invariant amplitudes F_i

$$F_1 = (-g_1 t + 2Mg_4)R^V(s, t) + (-g_1^c t + 2Mg_4^c)R_c(s, t), \\ F_2 = g_2 t R^A(s, t), \\ F_3 = (2Mg_1 - g_4)tR^V(s, t) + (2Mg_1^c - g_4^c)tR_c(s, t), \\ F_4 = 0. \quad (15)$$

We do not include cut contributions in the axial exchange amplitudes. In Eqs (15), $(g_1, g_2, g_4, g_1^c, g_4^c)$ are real parameters to be determined by fitting the data. Because of the connection with the one-particle exchange model they can be related to the products of $\gamma\pi^0$ and NN couplings of vectors and axial vectors [17]. Since matching between particle exchange and Regge amplitudes is only exact at the t -channel pole, the polynomial t dependence

in Eqs (15) is rather arbitrary, we keep it nevertheless to allow for more flexibility in describing the t -dependence.

The subscripts V and A in Eq. (15) specify the Regge trajectory $\alpha = \alpha_V(t)$ or $\alpha = \alpha_A(t)$ to be used in the Regge amplitudes of Eq. (11). We assume exchange degeneracy *i.e.* the same trajectory α_V for ω and ρ , and the same axial trajectory, α_A for b and h which, including the cut, we take to be linear,

$$\alpha_V(t) = \alpha_{V0} + \alpha'_V t, \quad \alpha_A(t) = \alpha_{A0} + \alpha'_A t, \\ \alpha_c(t) = \alpha_{c0} + \alpha'_c t. \quad (16)$$

Furthermore, from Eq. (10) it follows that for the $g_1 = \pm g_1^\rho + g_1^\omega$, $g_4 = \pm g_4^\rho + g_4^\omega$ and $g_2 = \pm g_2^b + g_2^h$ with the upper/lower sign referring the proton/neutron amplitudes, respectively. In addition to the five couplings we need to determine the six trajectory parameters $(\alpha_{V0}, \alpha'_V, \alpha_{A0}, \alpha'_A, \alpha_{c0}, \alpha'_c)$. Trajectory parameters are constrained by the meson mass-spin relations and are expected to be approximately given by [1]

$$\alpha_V(t) = 1 + 0.9(t - m_\rho^2) \quad \sim 0.5 + 0.9t \quad (17a)$$

$$\alpha_A(t) = 1 + 0.7(t - m_{b_1}^2) \quad \sim 0.7t \quad (17b)$$

In a simple model for Pomeron exchange [1], the Regge-Pomeron cut trajectory has an intercept, $\alpha_{c0} = \alpha_{V0}$ and a slope close to that of the Pomeron, *i.e.* we expect the cut trajectory to approximately give by

$$\alpha_c(t) \sim 0.5 + 0.2t. \quad (18)$$

IV. RESULTS

A. Data selection and interpretation

The t -channel exchanges govern in the physics of the s -channel region only for large energies and small angles. The exact region of validity of Regge theory will be deduced by analyzing the data. In the region $E_\gamma \geq 2$ GeV and $|t| < 3$ GeV² there are data on differential cross sections [18–22] shown in Fig. 1, the beam asymmetry [18], shown in Fig. 2, the ratio of differential cross section on neutron to proton targets [23, 24], shown in Fig. 2, and on target and recoil asymmetries [25–27], shown in Fig. 4.

The differential cross section in the energy range $E_\gamma = 6$ –15 GeV has a dip at $t \sim -0.5$ GeV². This value of momentum transfer is close to the wrong signature point of the vector trajectory *i.e.* $\alpha_V(t) = 0$. As explained in the previous section, vector exchange is expected to vanish at $\alpha_V = 0$ since it corresponds to a nonsense point, *i.e.* unphysical helicity coupling. The minimum seen in the data has therefore a clear interpretation within the Regge theory, however, a single Regge pole model would imply vanishing of the cross section at the non-sense point which is inconsistent with the data. The disappearance of the dip at lower energies, $E_\gamma \lesssim 2$ GeV can be used as signal for inapplicability of the simple Regge model. The

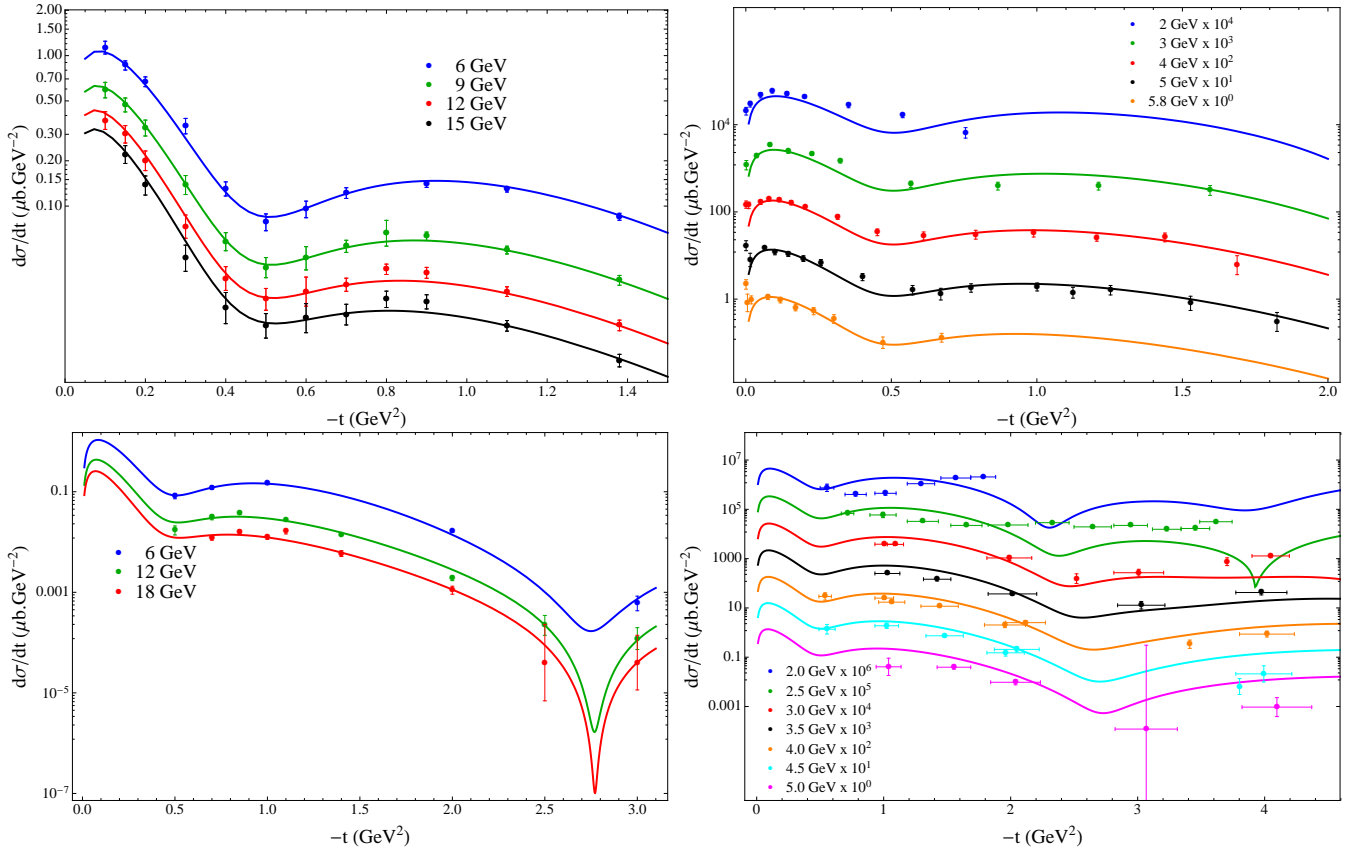


FIG. 1. (Color online). Differential cross section. Only the data in the region $E_\gamma \geq 4$ GeV and $\cos \theta_s \geq 0.6$ are used in the fit (see text). The model results in this region of are represented by solid lines. The dashed lines represent the extrapolation outside the fitting region. Data from [18–22].

data in the intermediate region $E_\gamma = 2 - 6$ GeV, however, does not give a precise determination of the energy where the simple Regge picture breaks down.

The beam asymmetry is sensitive to exchange on trajectories corresponding to mesons with negative naturalness, since it is given by

$$\Sigma = \frac{|\omega + \rho|^2 - |h + b|^2}{|\omega + \rho|^2 + |h + b|^2} \quad (19)$$

where each term corresponds to a single Regge amplitude. With the vector contribution being close to zero at $t \sim -0.5$ GeV², the beam asymmetry is predicted to be $\Sigma \sim -1$. In the other limit, with the axial vector being close to zero, $\Sigma = +1$ and deviations from this value measure the strength of the axial vector Regge trajectory contributions, as seen in Fig. 2. For not too large momentum transfers, $|t| < 2.5$ GeV², that value of α for the vector trajectory is larger than for the axial, $\alpha_V(t) > \alpha_A(t)$, cf. Eq. (17), thus as energy increases, the contribution of axial exchanges relative to vector exchanges decreases. The beam asymmetry is therefore expected to approach one as the energy increases. The data in Fig. 2, however, shows an approximately constant beam asymmetry as a function of energy.

The ratio of the differential cross sections on the neutron compared to the proton target also indicates presence of exchanges other than single Regge poles. This ratio is given by

$$\frac{d\sigma(n)/dt}{d\sigma(p)/dt} = \frac{|\omega - \rho|^2 + |h - b|^2}{|\omega + \rho|^2 + |h + b|^2}. \quad (20)$$

Since, phenomenologically it is observed that the isoscalar exchanges ω and h have trajectory slopes approximately equal to those of their vector partners, ρ and b , the ratio is expected to be relatively energy independent. The data shown in the right panel in Fig. 2 indicates a significant deviations from this expectation.

We conclude that qualitative features of the data are consistent with the single Regge pole approximations, however, quantitative description requires inclusion of other contributions, *e.g.* daughter trajectories or cuts.

B. Cut versus daughter

As discussed above, near the nonsense point $\alpha = 0$ ($t \sim -0.5$ GeV²), differential cross section is small but non-vanishing. Zero in the vector Regge exchange ampli-

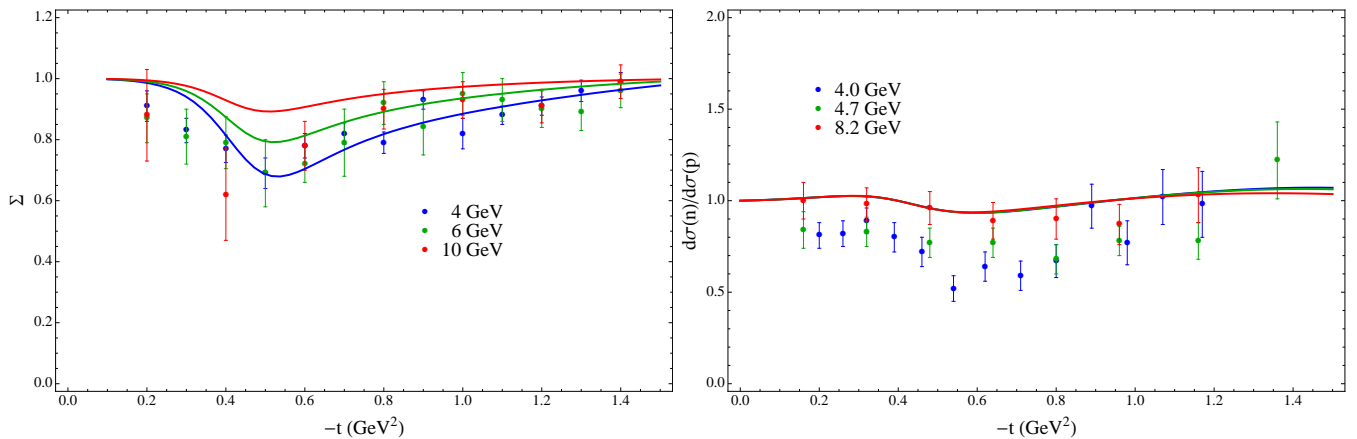


FIG. 2. (Color online). Beam asymmetry (left) and ratio of differential cross sections with neutron target to proton target (right). Data from [18] (left) and [23, 24] (right)

tude can be lifted by either axial Regge poles or corrections to the single Regge pole model. In order to determine which contribution dominates over the vector exchange we compare energy dependence of the differential cross section at $t = -0.5$ GeV² to that at $t = -0.1$ GeV², where the vector pole is expected to dominate. For the axial or daughter trajectory this ratio would decrease with energy since both have an intercept which is smaller than that of the vector trajectory. On the other hand, if it is a Regge-Pomeron cut the ratio would, up to logarithmic corrections, be approximatively energy independent since the intercept of the cut is similar to that of the pole, *cf.* Eq. (11). The measured ratio between differential cross sections at these two values of momentum transfer is 6.9%, 6.6% and 6.5% at $E_\gamma = 6, 9$ and 12 GeV, respectively. This is almost energy independent and we conclude that cuts might be more relevant than sub-leading Regge poles in filling up the zero at $t \sim -0.5$ GeV². Another discriminator between cuts and poles is the t -dependence. The logarithmic slope shown in Fig. 1, in the region $t \in [-0.1, -0.4]$ GeV² where the pole dominates is larger than that in the region $t \in [-0.9, -1.4]$ GeV². Since cut has a smaller slope than a pole we conclude that at the larger value of $|t|$ where the leading pole is suppressed it is the cut that dominated the differential cross section. To illustrate the difference between the vector-Regge-Pomeron cut model and a model with a sub-leading pole we compare their predictions for the differential cross section. In π^0 photoproduction, as shown later, the dominant Regge-pole contribution comes from the ω exchange, which is predominantly helicity-non-flip at the nucleon vertex in the s -channel. We thus place the ω contribution into the A_4 amplitude and take,

$$F_1 = 2Mg_4^p R(\alpha_V) + 2Mg_4^c R(\alpha_c) \quad (21a)$$

$$F_3 = -tg_4^p R(\alpha_V) - tg_4^c R(\alpha_c) \quad (21b)$$

with $g_4^p = 1$ and $g_4^c = 0.1$, representing a 10% contribution of the ω -Pomeron cut at the amplitude level. For a

model with a daughter trajectory, we take

$$F_1 = 2Mg_4^p R(\alpha_V) + 2Mg_4^d R(\alpha_d) \quad (22a)$$

$$F_3 = -tg_4^p R(\alpha_V) - tg_4^d R(\alpha_d) \quad (22b)$$

with $g_4^p = 1$ and $g_4^d = 0.5$. The couplings were chosen so that both models yield comparable cross sections.

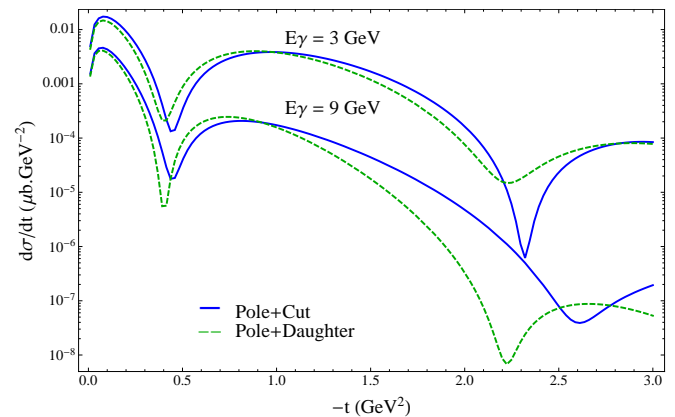


FIG. 3. (Color online). The two simple models discussed in the text for a beam energy of 3 and 9 GeV.

The predicted differential cross section for the two models at two photon energies $E_\gamma = 3$ and 9 GeV is shown in Fig. 3. As expected, the logarithmic slope in the range $1 \text{ GeV}^2 < |t| < 2 \text{ GeV}^2$ is different in the two models, the cut resulting in a smaller slope and dominating in this region of momentum transfer. Both models, have the first minimum coinciding with zero of the ω Regge pole but the energy dependence of the zero is different. Specifically, the ratio between the first maximum, at around $t = -0.1$ GeV² and the first minimum, at around $t = -0.4$ GeV² is almost energy independent for the model with the cut. The weak energy dependence of the dip and the smaller logarithmic slope at larger momentum transfers of the model with the cut make it phe-

nomenologically more appealing compared to the model with an additional pole.

We also note, that in the model with the cut, the position of the second dip, around $|t| \sim 2.2 - 2.6 \text{ GeV}^2$ seems to move with energy more than in the model with a second pole. With the existing data it is not possible to test this prediction, however, it might be possible with the forthcoming CLAS data [3].

C. Fitting procedure

The parameters of the Regge model from Sec. III are determined as follows. First we fix the vector Regge pole and the associated Regge cut parameters by fitting the differential cross section of photoproduction on the proton target. This does not determine the isospin of the vector exchange. The axial vector pole contribution to the differential cross section is small, (*cf.* Sec. IV B) and in the fit to the cross section it is ignored. The axial vector Regge pole parameters are determined by fitting the beam asymmetry, once the vector exchanges are fixed by the differential cross section. The target and recoil asymmetries are not included in the fits and constitute a prediction of the model.

We include in the fit the data from [18] and [19] in the kinematical range $E_\gamma \geq 6 \text{ GeV}$ and for $\cos\theta_s \geq 0.6$. We also include data from [24] and [22] for $E_\gamma \geq 4 \text{ GeV}$ and $\cos\theta_s \geq 0.6$. We exclude the very forward region $|t| < 0.01 \text{ GeV}^2$ since it is dominated by the Primakoff process². We do not include the data from [20], which is compatible with the other data, but has much wider t -bins and no data points close to the forward direction. We have found that the lower energy data $E_\gamma < 4 \text{ GeV}$ results in a significantly larger $\chi^2/\text{d.o.f.}$ compared to the other sets. Therefore we fix model parameters using data above 4 GeV and predict the cross section in the lower energy range $E_\gamma < 4 \text{ GeV}$. For $E_\gamma \geq 4 \text{ GeV}$ the model reproduces the data in the whole range of $|t| \leq 3 \text{ GeV}^2$. Overall the fit results in $\chi^2/\text{d.o.f.} = 3.43$ and for the parameters of the vector pole and cut are found (with α' in GeV^{-2})

$$g_1 = 1.24 \pm 1.56 \text{ GeV}^{-4}, \quad \alpha_{V0} = 0.54 \pm 0.03 \quad (23a)$$

$$g_4 = -6.68 \pm 0.80 \text{ GeV}^{-3}, \quad \alpha'_V = 1.34 \pm 0.08 \quad (23b)$$

$$g_1^c = -2.36 \pm 0.36 \text{ GeV}^{-4}, \quad \alpha_{c0} = 0.43 \pm 0.03 \quad (23c)$$

$$g_4^c = -4.26 \pm 0.99 \text{ GeV}^{-4}, \quad \alpha'_c = 0.16 \pm 0.01. \quad (23d)$$

Although we did not constrain parameters of the trajectories, the fit finds the vector trajectory consistent with expectations, *cf.* Eq. (17).

With the vector Regge pole and cut parameters determined using the high-energy data, in Fig. 1 we compare

model prediction with the data in the lower-energy region, $E_\gamma \geq 2 \text{ GeV}$. The model (solid lines) is extrapolated outside the fitting region (*i.e.* outside $E_\gamma \geq 4 \text{ GeV}$ and $\cos\theta_s \geq 0.6$) (dashed lines). It appears that the simple Regge pole plus a cut is qualitatively consistent with the data outside this region up to $t = -3 \text{ GeV}^2$, although the data in this region is rather sparse and it is impossible to clearly identify the region of applicability of the Regge theory.

As discussed in Sec. IV A, we assume that the main contribution to beam asymmetry comes from the axial vector Regge poles. From a fit to the beam asymmetry in the energy range $4 \leq E_\gamma(\text{GeV}) \leq 10$ with the vector Regge exchanges fixed by Eq. (23) we find

$$g_2 = -9.74 \pm 2.96 \text{ GeV}^{-4}, \quad (24a)$$

$$\alpha_{A0} = -0.22 \pm 0.33 \quad (24b)$$

$$\alpha'_A = 1.08 \pm 0.21 \text{ GeV}^{-2}. \quad (24c)$$

with $\chi^2/\text{d.o.f.} = 1.78$. The large uncertainty obtained for the intercept is not surprising. It originates from the discrepancy in the energy dependence between the data and the model with a single axial pole *cf.* Sec. IV A.

Since the differential cross section and the beam asymmetry do not discriminate between isovector and isoscalar Regge poles the coupling parameters in Eq. (23) are the sum of the two exchanges. The helicity flip and non-flip pole residues in the s -channel are proportional to g_1 and g_4 respectively. If we assume that in the s -channel the ω trajectory is dominantly helicity non-flip so that, $g_4 = g_4^\omega$, the ρ trajectory is helicity flip, *i.e.* $g_1 = g_1^\rho$ [1], and we neglect the h trajectory, *i.e.* $g_2 = g_2^b$, we can make a prediction for the ratio of the differential cross section on the neutron and proton targets. The two are related by a sign change in g_1 and g_2 *cf.* Eq. (10). A better agreement with the data is found if we consider the cut couplings to be both induced by a Pomeron- ω exchange, *i.e.* we do not flip the sign of g_1^c and g_4^c for a neutron target. We compare this prediction with the data [23, 24] in the energy range $4 \leq E_\gamma(\text{GeV}) \leq 8.2$ in Fig. 2. The angular distribution of the data is well reproduced by our theoretical prediction. However, as we already commented in Sec. IV A, the energy dependence of our model is only qualitatively consistent with the data. The degeneracy between ω and ρ trajectories produced a ratio of the differential cross section on the neutron and proton targets independent of the energy.

The target [25, 26] and recoil asymmetries [27] are compared to the data in Fig. 4. The two target asymmetry measurements [25, 26] were both performed at $E_\gamma = 4 \text{ GeV}$. The two data sets are not completely compatible, the data from Ref. [25] being somehow below the data from Ref. [26] at small momentum transfers. However, the data presented on Fig. 3 in the original publication [25] present a minimum $T \geq -0.7$ where the data from the same publication taken from the Durham data, displayed on the left panel in Fig. 4, extend to lower values $T \geq -0.8$. We do not have an explanation for this

² For a parametrization of the Primakoff effect in neutral pion photoproduction see Refs [9] and [28].

discrepancy. Concerning the recoil asymmetry, the data from Ref. [27] are given in the energy range from $E_\gamma = 4.1$ GeV to $E_\gamma = 6.3$ GeV and we compare with model predictions at $E_\gamma = 4, 5$ and 6 GeV. The target and recoil asymmetries are compatible with each other indicating that amplitude F_4 is small *cf.* Eq. (7). Although, in the recoil asymmetry, there is a structure around $t \sim -0.5$ GeV² absent in the target asymmetry. As emphasized by Berger and Fox [29], polarization observables provide crucial information on amplitudes and can discriminate between different high energy models. In our case, accurate measurements on both R and T polarization observables would improve our knowledge on the poorly known F_4 amplitude. Since we have set $F_4 = 0$ the target and recoil asymmetries in Eq. (7) are equal and proportional to $\text{Im } F_3 F_1^*$. Non-vanishing imaginary part requires at least two amplitudes are present, *e.g.* a pole and a cut. Since the vector exchange produces a zero at the nonsense point $\alpha = 0$ our model predicts that both asymmetries change sign at $t = -0.4$ GeV², which is qualitatively consistent with the data.

Beside the inclusion of the F_4 amplitudes, there is another possibility to improve the agreement with the recoil and target polarization data. It might happen that one of the vector poles, ω or ρ , does not have a wrong signature zero in one or both residues (F_1 and/or F_3). In this case the contribution of that particular exchange would not vanish at $\alpha_V = 0$. In Sec. III we have explained that the wrong signature point $\alpha = 0$ is a non-sense point and used this observation to justify a zero of the amplitude. This theoretical expectation should in principle be verified, for example via FESR. For example, a wrong signature zero is present in the ρ pole amplitude in pion-nucleon scattering and consistent with FESR [30]. This zero implies a dip in the differential cross section in $\pi^- p \rightarrow \pi^0 n$. The dip in $\gamma p \rightarrow \pi^0 p$ was therefore also assumed to come from the wrong signature zero. However the theoretical statement used in Sec. III to justify the wrong signature zero equally applies to η photoproduction. Since the neutral pion and eta photoproduction share the same t -channel exchanges, the fact that a dip is not observed in the differential cross section in $\gamma p \rightarrow \eta p$ [31] indicates that corrections to the pole approximation are stronger in photoproduction and could fill in the non sense zeros. Our model for the t -dependence of the poles and cuts, like any other models, has to be checked eventually against analyticity constraints, *i.e.* FESR. We hope that FESR in photoproduction, providing constraints on the residues, will shed more light and possibly solve the issues in polarization observables at high energies.

It has been argued in Ref. [32] that the interference between ρ and ω exchanges properly describes the target and recoil asymmetry. The authors of Ref. [32] used a rotating phase for the ρ pole, *i.e.* $R \propto \exp(-i\pi\alpha)$ instead of the signature factor, *i.e.* $R_\rho \propto 1 - \exp(-i\pi\alpha)$. The rotating phase emerges as a result of adding two degenerated Regge poles with opposite signature. This happens, for example in charged pion photoproduction where the

a_2 and ρ exchanges compensate mutually. More explicitly

$$R_{a_2} - R_\rho \propto (1 + e^{-i\pi\alpha}) - (1 - e^{-i\pi\alpha}) = 2e^{-i\pi\alpha}. \quad (25)$$

However charge conjugation in neutral pion photoproduction prevents the exchange of the degenerate partners of the ρ and ω poles (the a_2 and f_2 poles). Therefore the use of rotating (or constant) phase in neutral pion photoproduction is not justifiable on first principles. The only possibility for producing an interference between ω and ρ pole in polarization observables is a non degeneracy between their trajectories. This could possibly be investigated when more data on neutron target is provided.

We add for completeness that a weak-Regge-cut model failed to reproduce the target asymmetry as well [33]

We conclude this section with comparison, shown in Fig. 5, of the differential cross section computed using the exact expression and the high-energy approximation given by Eq. (8) and Eq. (7), respectively. We observe that the high-energy limit is a good approximation even at the lowest energies considered in the fits. The discrepancy increases as $|t|$ grows, for example, at $E_\gamma = 6$ GeV, and $t = -1$ GeV² the difference is approximately 12%.

V. PREDICTIONS

We give predictions of the model at various beam energies in Fig. 6. The energy range $E_\gamma = 3 - 6$ GeV corresponds to the recent CLAS measurement [3]. We also give a prediction for higher energy $E_\gamma = 9$ GeV relevant for the forthcoming measurements at GlueX. We show the differential cross section both as a function of momentum transfer and the s -channel scattering angle in the range $|t| < 3$ GeV². In the description of the model we repeatedly emphasized the role of zeros in Regge pole residues, *cf.* Eq. (11). These correspond to nonsense points, with α equal to non-positive integer. The first zero appears in the vector trajectory, at $\alpha_V = 0$, and is well established empirically, seen as a dip in the differential cross section at $t \sim -0.5$ GeV².

At larger $|t|$, zeros corresponding to lower integer values of Regge trajectories should become visible. For the vector trajectory, $\alpha_V(t) = -2$ corresponds to $t \sim -1.9$ GeV² and zero of the cut, $\alpha_c(t) = 0$ arises at $t \sim -2.75$ GeV². Since the cut dominates over the pole for large momentum transfers we expect the differential cross section to dip in this region of momentum transfer. Indeed for energies above $E_\gamma = 4$ GeV, the dip appears, *cf.* Fig. 6, around $t \sim -2.75$ GeV². There are however only a few data points at large $|t|$ to make a detailed comparison with the model. The second minimum in the differential cross section can therefore be used to discriminate between various models for the subleading Regge contributions interfering with the dominant vector pole. In the energy range $E_\gamma = 4 - 5.5$ GeV, the second dip should arise at angle $\theta \sim 60^\circ - 80^\circ$, and should be visible in the CLAS data [3].

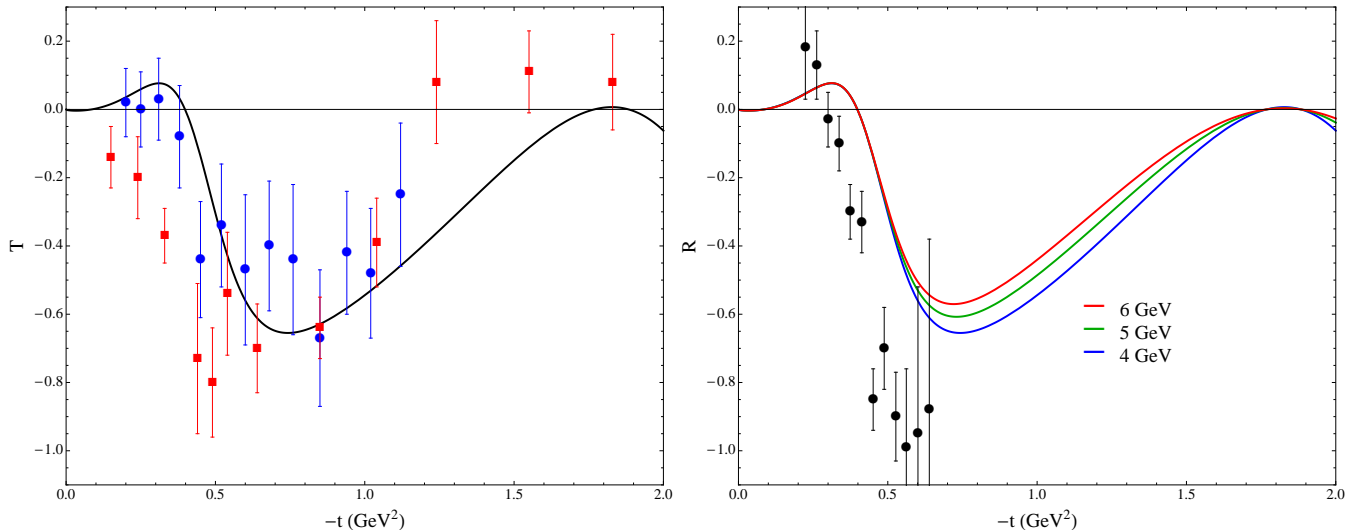


FIG. 4. (Color online). Target asymmetry at $E_\gamma = 4$ GeV from [25, 26] (left) and recoil asymmetry from [27] (right).

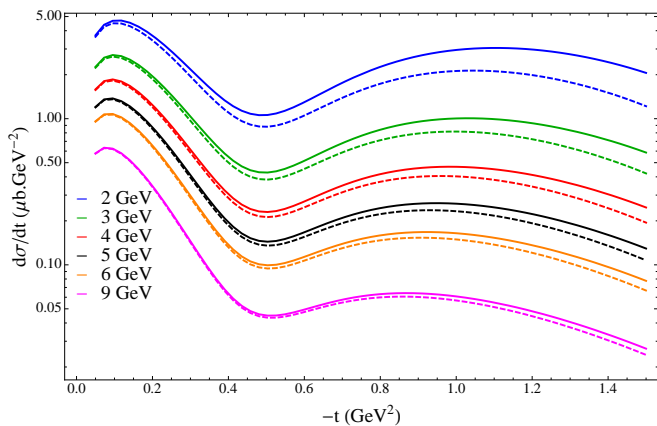


FIG. 5. (Color online). Comparison of differential cross section between the high energy limit Eq. (7) (solid lines) and the full expression Eq. (8) (dashed lines) for a wide range in incident beam energies.

VI. CONCLUSION

We investigated photoproduction of neutral pions for energies above s -channel resonance region. Our amplitudes include the leading Regge poles in the t -channel and describe well the differential cross section for beam energies above 4 GeV and for small scattering angles $\cos \theta_s \geq 0.6$. The first dip seen at $t \sim -0.5$ GeV^2 , is characteristic to the vector Regge pole and seems to persist down to $E_\gamma = 3$ GeV although the quantitative analysis is not possible given the quality of the data in the intermediate energy region 3 – 4 GeV. Below $E_\gamma = 3$ GeV nucleon resonances become visible and were the focus of most of the recent efforts in pion photo production [5–8]. These studies could benefit from the results of the higher energy data analysis, for example by implementing finite- t or finite energy sum rule constraints on the resonance

models. The resulting baryon spectrum from the analysis in Refs [7, 8] is compared in Ref. [34]. A common agreement is found for the lowest nucleon excitations, but both spectra strongly disagree in the center-of-mass energies 1.7 – 2.0 GeV. We hope that our amplitudes will provide significant insights in the baryon spectrum to solve the remaining ambiguities in this topic. The sum rules for pion photoproduction were studied in the past [4, 35–37], however, only now precise partial waves for the low energy data are available.

In Sec. IV A we analyzed the energy dependence of the beam asymmetry for the reaction $\gamma p \rightarrow \pi^0 p$ and the differential cross section for the reaction $\gamma n \rightarrow \pi^0 n$. Based on the expected trajectories for the ω, ρ and the b poles and the dominance of these Regge poles, we concluded that the beam asymmetry should approach one as the energy increases and the differential cross section for $\gamma n \rightarrow \pi^0 n$ should have the same energy dependence as for the reaction $\gamma p \rightarrow \pi^0 p$. Both are only qualitatively reproduced, however, the data for these observables at high energies is rather sparse and we hope that more precise data, including the forthcoming data from CLAS, and the implementation of analyticity constraints will help clarifying these issues.

All the material, including data and software are available in an interactive from online [38]. We invite the interested readers to contact the authors.

ACKNOWLEDGMENTS

We thank R. Workman for his help in developing the website. We acknowledge I. Strakovsky and M. Amarian for discussions concerning forthcoming CLAS data. This material is based upon work supported in part by the U.S. Department of Energy, Office of Science, Office of Nuclear Physics under contract DE-AC05-06OR23177.

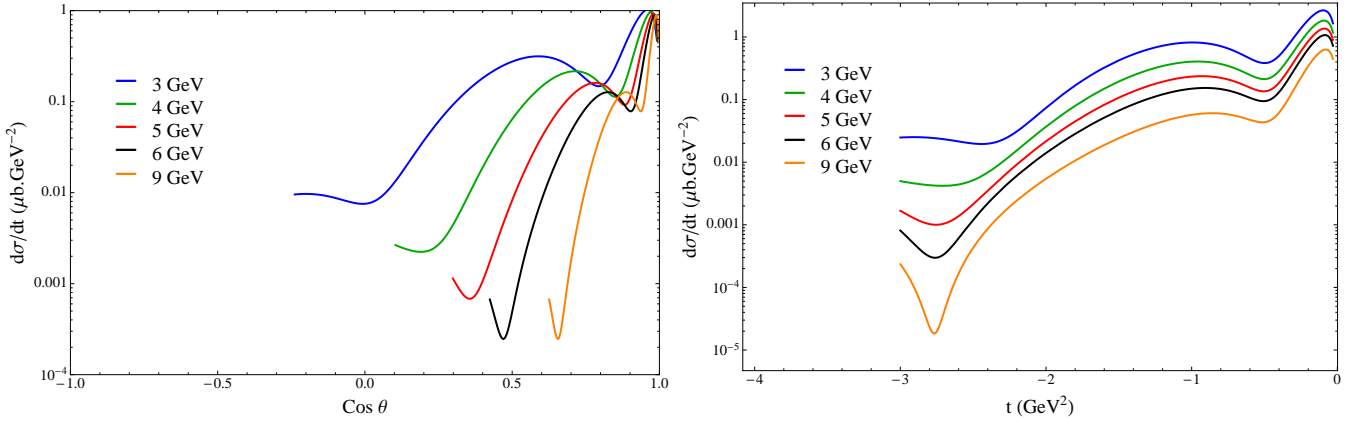


FIG. 6. Model prediction (solid lines) for the differential cross section at CLAS and GlueX energies. The dashed lines represent the extrapolation outside the region ($E_\gamma \geq 4$ GeV, $\cos \theta_s \geq 0.6$).

This work was also supported in part by the U.S. Department of Energy under Grant No. DE-FG0287ER40365, National Science Foundation under Grant PHY-1415459.

Appendix A: t -channel helicity amplitudes

In this Appendix we compute the combinations of scalar amplitudes with good quantum numbers of the t -channel $\gamma(k)\pi^0(-q) \rightarrow \bar{N}(-p_2)N(p_4)$. The Mandelstam variables $s = (k + p_2)^2$, $t = (k - q)^2$, $u = (k - p_4)^2$ are related through $s + t + u = 2M^2 + \mu^2$. In the t -channel, the physical domain of the Mandelstam variable is ($t \geq 4M^2$, $s \leq 0$).

We start by decomposing the t -channel helicity amplitudes in the tensor basis [11].

$$A_{\lambda_4 \lambda_2, \lambda_1}^t(s, t) = \bar{u}_{\lambda_4}(p_4) \sum_{i=1}^4 A_i(s, t) M_i v_{\lambda_2}(-p_2). \quad (\text{A1})$$

where A_i are scalar functions and

$$M_1 = \frac{1}{2} \gamma_5 \gamma_\mu \gamma_\nu F^{\mu\nu}, \quad (\text{A2a})$$

$$M_2 = 2\gamma_5 q_\mu p_\nu F^{\mu\nu}, \quad (\text{A2b})$$

$$M_3 = \gamma_5 \gamma_\mu q_\nu F^{\mu\nu}, \quad (\text{A2c})$$

$$M_4 = \frac{i}{2} \varepsilon_{\alpha\beta\mu\nu} \gamma^\alpha q^\beta F^{\mu\nu}, \quad (\text{A2d})$$

with $p = (p_2 + p_4)/2$. The tensors $F^{\mu\nu} = \epsilon^\mu(k, \lambda_1)k^\nu - k^\mu \epsilon^\nu(k, \lambda_1)$ satisfy gauge invariance by construction.

In the t -channel center of mass frame,

$$\begin{aligned} k^\mu &= (k_t, 0, 0, k_t), & p_2^\mu &= (-E_N^t, -p_t \sin \theta_t, 0, -p_t \cos \theta_t), \\ q^\mu &= (-E_\pi^t, 0, 0, k_t), & p_4^\mu &= (+E_N^t, -p_t \sin \theta_t, 0, -p_t \cos \theta_t). \end{aligned} \quad (\text{A3})$$

The first component is the energy and the metric is $\text{diag}(+, -, -, -)$. E_N^t and E_π^t are the nucleon and pion

energies. The scattering angle in the t -channel is θ_t . p_t is the momentum of the nuclei in their rest frame. In this frame, k_t is the photon and pion momenta. The masses of the pion and the nucleon are respectively μ and M . The kinematical quantities are

$$E_\pi^t = (t + \mu^2)/2\sqrt{t}, \quad E_N^t = \sqrt{t}/2 \quad (\text{A4a})$$

$$p_t = \sqrt{t/4 - M^2}, \quad k_t = (t - \mu^2)/2\sqrt{t} \quad (\text{A4b})$$

$$\cos \theta_t = \frac{s - u}{4k_t p_t}, \quad \sin \theta_t = \frac{\sqrt{\phi/t}}{2k_t p_t}, \quad (\text{A4c})$$

with $\phi = stu - \mu^2 M^2 (\mu^2 - t) - t M^4 > 0$. In the s -channel physical region we use the convention of Trueman and Wick Ref. [39], and evaluate the square root with the prescription $s \rightarrow s + i\epsilon$ and $t \rightarrow t - i\epsilon$. It is useful to remember that, in the s -channel, E_N^t , k_t and p_t are purely imaginary with a negative imaginary part, $\cos \theta_t$ is real and negative and $\sin \theta_t$ is imaginary with a positive imaginary part.

For the spinors, we use the Dirac representation. The γ -matrices are, with σ_i the Pauli matrices,

$$\gamma^0 = \begin{pmatrix} 1_2 & 0 \\ 0 & -1_2 \end{pmatrix}, \quad \gamma^i = \begin{pmatrix} 0 & \sigma^i \\ -\sigma^i & 0 \end{pmatrix}, \quad \gamma^5 = \begin{pmatrix} 0 & 1_2 \\ 1_2 & 0 \end{pmatrix}. \quad (\text{A5})$$

For the evaluation of Eq. (A1), the spinors are (with the lower-script $\pm \equiv \pm \frac{1}{2}$)

$$\begin{aligned} v_+(-p_2) &= \begin{pmatrix} -\sqrt{E_N^t - M} \chi_2(\theta_t) \\ \sqrt{E_N^t + M} \chi_2(\theta_t) \end{pmatrix}, \\ v_-(-p_2) &= \begin{pmatrix} -\sqrt{E_N^t - M} \chi_1(\theta_t) \\ -\sqrt{E_N^t + M} \chi_1(\theta_t) \end{pmatrix}, \end{aligned} \quad (\text{A6})$$

$$\begin{aligned} \bar{u}_+(p_4) &= (\sqrt{E_N^t + M} \chi_2^\dagger(\theta_t) \quad -\sqrt{E_N^t - M} \chi_2^\dagger(\theta_t)), \\ \bar{u}_-(p_4) &= (\sqrt{E_N^t + M} \chi_1^\dagger(\theta_t) \quad \sqrt{E_N^t - M} \chi_1^\dagger(\theta_t)), \end{aligned}$$

with

$$\chi_1(\theta) = \begin{pmatrix} \cos \theta/2 \\ \sin \theta/2 \end{pmatrix}, \quad \chi_2(\theta) = \begin{pmatrix} -\sin \theta/2 \\ \cos \theta/2 \end{pmatrix}, \quad (\text{A7})$$

and the polarization tensor for the photon is $\epsilon^\mu(k, \pm 1) = (0, \mp 1, -i, 0)/\sqrt{2}$.

With these definition the t -channel amplitudes can be expressed in terms of the scalar amplitudes and the kinematical quantities,

$$\begin{aligned} A_{++1}^t &= \sqrt{2}k_t \frac{\sin \theta_t}{2} \left[\sqrt{t}(A_1 - 2MA_4) - 2p_t(A_1 + tA_2) \right] \\ A_{--1}^t &= \sqrt{2}k_t \frac{\sin \theta_t}{2} \left[\sqrt{t}(A_1 - 2MA_4) + 2p_t(A_1 + tA_2) \right] \\ A_{+-1}^t &= \sqrt{2}k_t \sin^2 \frac{\theta_t}{2} \left[2p_t \sqrt{t}A_3 - (2MA_1 - tA_4) \right] \\ A_{-+1}^t &= \sqrt{2}k_t \cos^2 \frac{\theta_t}{2} \left[-2p_t \sqrt{t}A_3 - (2MA_1 - tA_4) \right] \end{aligned} \quad (\text{A8})$$

The amplitudes with negative photon helicity are obtained from the relations

$$A_{\pm\pm,-1}^t = A_{\mp\mp,1}^t, \quad A_{\pm\mp,-1}^t = -A_{\mp\pm,1}^t. \quad (\text{A9})$$

In Eq. (A8), the invariant amplitudes A_i contain dynamical singularities. Some of the kinematical singularities in t are explicitly extracted (and arise in p_t, k_t and \sqrt{t}). All kinematical singularities in the variable s are encoded in the trigonometric functions. They arise from the spin of the external particles and are independent of the exchanged particle. They can be extracted easily from the partial wave decomposition in the t -channel

$$A_{\lambda_4\lambda_2,\lambda_1}^t(s, t) = \sum_{J=1}^{\infty} (2J+1) T_{\lambda'\lambda}^J(t) d_{\lambda'\lambda}^J(z_t). \quad (\text{A10})$$

with $\lambda = \lambda_1 - \lambda_3 = \lambda_1$, $\lambda' = \lambda_2 - \lambda_4$ and $z_t = \cos \theta_t$. The Wigner rotation function $d_{\lambda'\lambda}^J(z_t) = \xi_{\lambda'\lambda}(z_t) P_{\lambda'\lambda}^J(z_t)$, where P^J is a polynomial, has indeed a cut in the s variable. They originate from the half-angle factor

$$\xi_{\lambda'\lambda}(z_t) = \left(\frac{1-z_t}{2} \right)^{\frac{1}{2}|\lambda'-\lambda|} \left(\frac{1+z_t}{2} \right)^{\frac{1}{2}|\lambda'+\lambda|}. \quad (\text{A11})$$

The partial waves $T_{\lambda'\lambda}^J$ have a well defined spin J but are not eigenstate of parity. The good parity combinations are $T_{\lambda'\lambda}^J \pm T_{\lambda'\lambda}^J$. In order to form parity conserving amplitudes free of kinematical singularities, one first needs to remove the half-angle factor with the definition

$$A_{\lambda_4\lambda_2,\lambda_1}^t = \left[\cos \frac{\theta_t}{2} \right]^{|\lambda+\lambda'|} \left[\sin \frac{\theta_t}{2} \right]^{|\lambda-\lambda'|} \hat{T}_{\lambda\lambda'}. \quad (\text{A12})$$

Then t -channel parity conserving helicity amplitudes (PCHAs) are given by [12, 13]

$$\hat{T}_{\lambda\lambda'}^\eta = \frac{1}{\sqrt{2}} \left(\hat{T}_{\lambda\lambda} + \eta(-1)^{\lambda'} \hat{T}_{\lambda'-\lambda} \right). \quad (\text{A13})$$

η is called the naturality as it corresponds to $P(-)^J$ for an exchanged particle of parity P and spin J in the

t -channel. Using the expressions (A8), we obtain the relations between the PCHAs and the invariant amplitudes

$$\hat{T}_{01}^+ = -2k_t \sqrt{t}(-A_1 + 2MA_4) \quad (\text{A14a})$$

$$\hat{T}_{01}^- = -4p_t k_t (A_1 + tA_2) \quad (\text{A14b})$$

$$\hat{T}_{11}^+ = -2k_t (2MA_1 - tA_4) \quad (\text{A14c})$$

$$\hat{T}_{11}^- = 4p_t k_t \sqrt{t}A_3 \quad (\text{A14d})$$

The quantum numbers of the PCHAs are best computed using the standard non relativistic state $|J, M, L, S\rangle$, *cf.* Appendix of Ref. [40]. Using Eq. (B5) from [41], we can express the 2-nucleon state $|J, M; \lambda_4, \lambda_2\rangle$ as

$$\begin{aligned} \sqrt{2}|J, 0; \pm\pm\rangle &= \pm |J, 0, J, 0\rangle \\ &+ \left(\frac{J}{2J+1} \right)^{\frac{1}{2}} |J, 0, J-1, 1\rangle \\ &- \left(\frac{J+1}{2J+1} \right)^{\frac{1}{2}} |J, 0, J+1, 1\rangle, \end{aligned} \quad (\text{A15a})$$

$$\begin{aligned} \sqrt{2}|J, \pm 1; \pm\mp\rangle &= \mp |J, \pm 1, J, 1\rangle \\ &+ \left(\frac{J+1}{2J+1} \right)^{\frac{1}{2}} |J, \pm 1, J-1, 1\rangle \\ &+ \left(\frac{J}{2J+1} \right)^{\frac{1}{2}} |J, \pm 1, J+1, 1\rangle. \end{aligned} \quad (\text{A15b})$$

Since $|J, M, L, S\rangle$ have parity $(-1)^{L+1}$ and charge conjugation $(-1)^{L+S}$, the PCHAs are invariant under CP . In the above decomposition, only $|J, 0, J, 0\rangle$ has $CP = -1$. Introducing standard combinations of invariant amplitudes, we find that their quantum numbers are

$$F_1 = -A_1 + 2MA_4, \quad \eta = +1, \quad CP = +1, \quad (\text{A16a})$$

$$F_2 = A_1 + tA_2, \quad \eta = -1, \quad CP = -1, \quad (\text{A16b})$$

$$F_3 = 2MA_1 - tA_4, \quad \eta = +1, \quad CP = +1, \quad (\text{A16c})$$

$$F_4 = A_3, \quad \eta = -1, \quad CP = +1. \quad (\text{A16d})$$

Appendix B: s -channel helicity amplitudes and observables

We are interested in the observables for the photoproduction of a neutral pion at the leading order in the center of mass energy squared. The observables are functions of the s -channel amplitudes, defined by

$$A_{\mu_4, \mu_2 \mu_1}^s = \bar{u}_{\mu_4}(p_4) \sum_{i=1}^4 A_i M_i u_{\mu_2}(p_2). \quad (\text{B1})$$

In Walker's notation [35] we have ($W = \sqrt{s}$)

$$A_{+,+1}^s = (8\pi W)H_4, \quad A_{+,-1}^s = (8\pi W)H_3, \quad (\text{B2a})$$

$$A_{-,-1}^s = (8\pi W)H_1, \quad A_{-,+1}^s = (8\pi W)H_2. \quad (\text{B2b})$$

H_1 and H_4 are single spin flip amplitudes, H_2 is the non-flip amplitude and H_3 is the double flip amplitude.

We use SAID/MAID conventions for the observables [42]

$$\frac{d\sigma}{dt} = \frac{\pi}{k_s^2} \frac{1}{2} (|H_1|^2 + |H_2|^2 + |H_3|^2 + |H_4|^2), \quad (\text{B3a})$$

$$\Sigma \frac{d\sigma}{dt} = \frac{\pi}{k_s^2} \text{Re}(H_1 H_4^* - H_2 H_3^*), \quad (\text{B3b})$$

$$T \frac{d\sigma}{dt} = \frac{\pi}{k_s^2} \text{Im}(H_1 H_2^* + H_3 H_4^*), \quad (\text{B3c})$$

$$R \frac{d\sigma}{dt} = \frac{\pi}{k_s^2} \text{Im}(H_3 H_1^* + H_4 H_2^*). \quad (\text{B3d})$$

$k_s = (s - M^2)/2\sqrt{s} = ME_\gamma/\sqrt{s}$ is the photon momentum in the s -channel center of mass frame.

The s -channel amplitudes can be evaluated using an explicit representation for the spinors as we did in the previous section. In the s -channel region, the four vector

$$\begin{aligned} k_s^\mu &= (k_s, 0, 0, k_s), & q^\mu &= (E_\pi^s, q_s \sin \theta_s, 0, q_s \cos \theta_s), \\ p_2^\mu &= (E_2^s, 0, 0, -k_s), & p_4^\mu &= (E_4^s, -q_s \sin \theta_t, 0, -q_s \cos \theta_t). \end{aligned} \quad (\text{B4})$$

The kinematical quantities are

$$\begin{aligned} k_s &= (s - M^2)/2\sqrt{s}, & E_\pi^s &= (s - M^2 + \mu^2)/2\sqrt{s}, \\ E_2^s &= (s + M^2)/2\sqrt{s}, & E_4^s &= (s + M^2 - \mu^2)/2\sqrt{s}, \\ \cos \theta_s &= \frac{t - u + \Delta/s}{4k_s q_s}, & \sin \theta_s &= \frac{\sqrt{\phi/s}}{2k_s q_s}, \end{aligned} \quad (\text{B5})$$

with $\Delta = M^2(M^2 - \mu^2)$ and

$$q_s = [(s - (M + \mu)^2)(s - (M - \mu)^2)]^{\frac{1}{2}}/2\sqrt{s}. \quad (\text{B6})$$

For the evaluation of Eq. (B1), the spinors are

$$\begin{aligned} u_+(p_2) &= \begin{pmatrix} \sqrt{E_2^s + M} \chi_2(0) \\ \sqrt{E_2^s - M} \chi_2(0) \end{pmatrix}, \\ u_-(p_2) &= \begin{pmatrix} -\sqrt{E_2^s + M} \chi_1(0) \\ \sqrt{E_2^s - M} \chi_1(0) \end{pmatrix}, \\ \bar{u}_+(p_4) &= (\sqrt{E_4^s + M} \chi_2^\dagger(\theta_s) \quad -\sqrt{E_4^s - M} \chi_2^\dagger(\theta_s)), \\ \bar{u}_-(p_4) &= (\sqrt{E_4^s + M} \chi_1^\dagger(\theta_s) \quad \sqrt{E_4^s - M} \chi_1^\dagger(\theta_s)), \end{aligned} \quad (\text{B7})$$

and the polarization tensor for the photon is $\epsilon^\mu(k, \pm 1) = (0, \mp 1, -i, 0)/\sqrt{2}$.

The expression for the s -channel helicity amplitudes in terms of the CGLN invariant amplitudes A_i are quite lengthy. Their expressions are most conveniently expressed as function of other scalar amplitudes, the CGLN

\mathcal{F}_i . We obtain

$$H_1 = \frac{-1}{\sqrt{2}} \sin \theta_s \cos \frac{\theta_s}{2} (\mathcal{F}_3 + \mathcal{F}_4) \quad (\text{B8a})$$

$$H_3 = \frac{1}{\sqrt{2}} \sin \theta_s \sin \frac{\theta_s}{2} (\mathcal{F}_3 - \mathcal{F}_4) \quad (\text{B8b})$$

$$H_2 = \sqrt{2} \cos \frac{\theta_s}{2} (\mathcal{F}_2 - \mathcal{F}_1) + H_3 \quad (\text{B8c})$$

$$H_4 = \sqrt{2} \sin \frac{\theta_s}{2} (\mathcal{F}_2 + \mathcal{F}_1) - H_1 \quad (\text{B8d})$$

where

$$\mathcal{F}_1 = \frac{Z_2^+ Z_4^+}{8\pi W} \left[-(M - W)A_1 + \frac{\mu^2 - t}{2}(A_3 - A_4) + (M - W)^2 A_4 \right] \quad (\text{B9a})$$

$$\mathcal{F}_2 = \frac{Z_2^- Z_4^-}{8\pi W} \left[-(M + W)A_1 + \frac{\mu^2 - t}{2}(A_3 - A_4) + (M + W)^2 A_4 \right] \quad (\text{B9b})$$

$$\mathcal{F}_3 = q_s \frac{Z_2^- Z_4^+}{8\pi W} (M + W) \left[-(M - W)A_2 + (A_3 - A_4) \right] \quad (\text{B9c})$$

$$\mathcal{F}_4 = q_s \frac{Z_2^+ Z_4^-}{8\pi W} (M - W) \left[-(M + W)A_2 + (A_3 - A_4) \right] \quad (\text{B9d})$$

It worth noting that the amplitudes \mathcal{F}_i have kinematical singularities coming from the factors

$$Z_{2,4}^\pm = \sqrt{E_{2,4} \pm M}. \quad (\text{B10})$$

Another instructive method to obtain the s -channel amplitudes, given in [39], is to express them in terms of the t -channel using crossing relations. Of course, parity conserving combinations rotate independently

$$\begin{pmatrix} A_{+,+1}^s \pm A_{-,-1}^s \\ A_{+,-1}^s \mp A_{-,+1}^s \end{pmatrix} = -iR \left(\frac{\chi_2 \mp \chi_4}{2} \right) \begin{pmatrix} A_{+,+1}^t \pm A_{-,-1}^t \\ A_{+,-1}^t \mp A_{-,+1}^t \end{pmatrix}. \quad (\text{B11})$$

The rotation matrix is

$$R(\chi) = \begin{pmatrix} \cos \chi & \sin \chi \\ -\sin \chi & \cos \chi \end{pmatrix}, \quad (\text{B12})$$

and the crossing angles are

$$\begin{aligned} \cos \chi_2 &= -\frac{-st + M^2(\mu^2 - t)}{\lambda^{\frac{1}{2}}(s, 0, M^2)\lambda^{\frac{1}{2}}(t, 0, \mu^2)} \approx -\sqrt{\frac{-t}{4M^2 - t}}, \\ \cos \chi_4 &= \frac{(-t)(s - \mu^2) - M^2(t + 2\mu^2)}{\lambda^{\frac{1}{2}}(s, \mu^2, M^2)\lambda^{\frac{1}{2}}(t, M^2, M^2)} \approx \sqrt{\frac{-t}{4M^2 - t}}. \end{aligned} \quad (\text{B13})$$

The symbols \approx stands for the leading order in s and the triangle function is $\lambda(a, b, c) = a^2 + b^2 + c^2 - 2(ab + bc + ca)$.

Since the crossing matrix (B11) is a rotation (up to a global phase³), it preserves the norm. The differential cross section can be then computed directly with the t -channel amplitudes without performing the rotation. The result is

$$\begin{aligned} \frac{d\sigma}{dt} = \frac{1}{64\pi} \frac{|k_t|^2}{4M^2 E_\gamma^2} & \left[2|\sin\theta_t|^2 (|2p_t F_2|^2 - t|F_1|^2) \right. \\ & + (1 - \cos\theta_t)^2 |F_3 + 2\sqrt{t}p_t F_4|^2 \\ & \left. + (1 + \cos\theta_t)^2 |F_3 - 2\sqrt{t}p_t F_4|^2 \right]. \quad (\text{B14}) \end{aligned}$$

In the evaluation of the differential cross section with t -channel amplitudes, one has to remember that $\sin\theta_t$ is a complex number in the physical region of the process $\gamma p \rightarrow \pi^0 p$.

Single polarization observables Σ, T, R are best evaluated in the high energy limit. The error made by using this approximation are compensated by calculating the ratio of quadratic forms of amplitudes, cf. Eq. (B3). Keeping only the dominant term in s , the crossing rela-

tions take a simple form

$$\begin{aligned} \frac{1}{\sqrt{2}} \begin{pmatrix} H_4 + H_1 \\ H_3 - H_2 \end{pmatrix} & \approx \frac{W/8\pi}{4M^2 - t} \begin{pmatrix} 2M & \sqrt{-t} \\ -\sqrt{-t} & 2M \end{pmatrix} \begin{pmatrix} \sqrt{-t}F_1 \\ F_3 \end{pmatrix}, \\ \frac{1}{\sqrt{2}} \begin{pmatrix} H_4 - H_1 \\ H_3 + H_2 \end{pmatrix} & \approx \frac{W}{8\pi} \begin{pmatrix} 0 & 1 \\ -1 & 0 \end{pmatrix} \begin{pmatrix} F_2 \\ \sqrt{-t}F_4 \end{pmatrix}. \quad (\text{B15}) \end{aligned}$$

The apparent pole at $t = 4M^2$ in the first equation above is spurious and disappears when the scalar amplitudes A_i are substituted. We indeed obtain

$$\frac{1}{\sqrt{2}} \begin{pmatrix} H_4 + H_1 \\ H_3 - H_2 \end{pmatrix} \approx \frac{W}{8\pi} \begin{pmatrix} \sqrt{-t}A_4 \\ A_1 \end{pmatrix}. \quad (\text{B16})$$

The relations (B15) were derived in Ref. [15]. We corrected a sign mistake in the rotation matrix Eq. (2.3) in Ref. [15]. This mistake propagated through the observables. The reader could easily check that the pole $t = 4M^2$ does not cancel as it should in the observables Eq. (A.10)-(A.13) in Ref. [15]. The correct expressions at leading order in the energy squared are

$$\frac{d\sigma}{dt} \approx \frac{1}{32\pi} \left[\frac{|F_3|^2 - t|F_1|^2}{4M^2 - t} + |F_2|^2 - t|F_4|^2 \right] \quad (\text{B17a})$$

$$\Sigma \frac{d\sigma}{dt} \approx \frac{1}{32\pi} \left[\frac{|F_3|^2 - t|F_1|^2}{4M^2 - t} - |F_2|^2 + t|F_4|^2 \right] \quad (\text{B17b})$$

$$T \frac{d\sigma}{dt} \approx \frac{1}{16\pi} \sqrt{-t} \operatorname{Im} \left[\frac{F_3 F_1^*}{4M^2 - t} + F_4 F_2^* \right] \quad (\text{B17c})$$

$$R \frac{d\sigma}{dt} \approx \frac{1}{16\pi} \sqrt{-t} \operatorname{Im} \left[\frac{F_3 F_1^*}{4M^2 - t} - F_4 F_2^* \right] \quad (\text{B17d})$$

-
- [1] A. Irving and R. Worden, Phys.Rept. **34**, 117 (1977).
[2] R. Worden, Nucl.Phys. **B37**, 253 (1972).
[3] CLAS collaboration, in preparation.
[4] R. Odorico, Nucl.Phys. **B101**, 480 (1975).
[5] D. Drechsel, S. Kamalov, and L. Tiator, Eur.Phys.J. **A34**, 69 (2007), 0710.0306.
[6] R. L. Workman, W. J. Briscoe, M. W. Paris, and I. I. Strakovsky, Phys.Rev. **C85**, 025201 (2012), 1109.0722.
[7] A. Anisovich, R. Beck, E. Klempt, V. Nikonov, A. Sarantsev, et al., Eur.Phys.J. **A48**, 88 (2012), 1205.2255.
[8] H. Kamano, S. Nakamura, T. S. H. Lee, and T. Sato, Phys.Rev. **C88**, 035209 (2013), 1305.4351.
[9] A. Sibirtsev, J. Haidenbauer, S. Krewald, U. Meissner, and A. Thomas, Eur.Phys.J. **A41**, 71 (2009), 0902.1819.
[10] V. N. Gribov, Y. L. Dokshitzer, and J. Nyiri (2009).
[11] G. Chew, M. Goldberger, F. Low, and Y. Nambu, Phys.Rev. **106**, 1345 (1957).
[12] P. Collins, *Regge Theory and High Energy Physics* (Cambridge Monograph on Mathematical Physics, 1977).
[13] A. Martin and S. T. D., *Elementary Particle Theory* (Noth-Holland, 1970).
[14] J. Ader, M. Capdeville, and P. Salin, Nucl. Phys. **B3**, 407 (1967).
[15] I. Barker, A. Donnachie, and J. Storrow, Nucl.Phys. **B79**, 431 (1974).
[16] P. Collins, Phys.Rept. **1**, 103 (1971).
[17] B. G. Yu, T. K. Choi, and W. Kim, Phys.Rev. **C83**, 025208 (2011), 1103.1203.
[18] R. L. Anderson, D. Gustavson, J. Johnson, I. Overman, D. Ritson, et al., Phys.Rev. **D4**, 1937 (1971).
[19] B. Barish, R. Gomez, D. Kreinick, C. Peck, J. Pine, et al., Phys.Rev. **D9**, 566 (1974).
[20] G. Bolon, C. Garelick, S. Homma, R. Lewis, W. Lobar, et al., Phys.Rev.Lett. **18**, 926 (1967).
[21] W. Braunschweig, W. Erlewein, H. Frese, K. Luebelsmeyer, H. Meyer-Wachsmuth, D. Schmitz, and A. Schultz Von Dratzig, Nucl. Phys. **B51**, 167 (1973).
[22] R. L. Anderson, D. Gustavson, D. Ritson, G. Weitsch, H. Halpern, et al., Phys.Rev. **D14**, 679 (1976).
[23] A. Osborne, A. Brownam, K. Hanson, W. Meyer, A. Silberman, et al., Phys.Rev.Lett. **29**, 1621 (1972).

³ This phase is present in the original calculation in Ref. [39] but was overlooked in subsequent publications. See for instance Ref. [12].

- [24] W. Braunschweig, H. Dinter, W. Erlewein, H. Frese, K. Luebelsmeyer, et al., Nucl.Phys. **B51**, 157 (1973).
- [25] P. Booth, G. Court, B. Craven, R. Gamet, P. Hayman, et al., Phys.Lett. **B38**, 339 (1972).
- [26] H. Bienlein, W. Braunschweig, H. Dinter, W. Erlewein, H. Frese, et al., Phys.Lett. **B46**, 131 (1973).
- [27] M. Deutsch, L. Golub, P. Kijewski, D. Potter, D. Quinn, et al., Phys.Rev.Lett. **29**, 1752 (1972).
- [28] J. M. Laget, Phys. Rev. **C72**, 022202 (2005), hep-ph/0502233.
- [29] E. L. Berger and G. Fox, Phys.Rev.Lett. **25**, 1783 (1970).
- [30] V. Mathieu, I. V. Danilkin, C. Fernández-Ramírez, M. R. Pennington, D. Schott, A. P. Szczepaniak, and G. Fox (2015), 1506.01764.
- [31] W. Braunschweig, W. Erlewein, H. Frese, K. Luebelsmeyer, H. Meyer-Wachsmuth, D. Schmitz, A. Schultz Von Dratzig, and G. Wessels, Phys. Lett. **B33**, 236 (1970).
- [32] M. Guidal, J. Laget, and M. Vanderhaeghen, Nucl.Phys. **A627**, 645 (1997).
- [33] G. R. Goldstein and J. F. Owens, Phys. Rev. **D7**, 865 (1973).
- [34] M. Pennington, EPJ Web Conf. **73**, 01001 (2014), 1402.5406.
- [35] R. Walker, Phys.Rev. **182**, 1729 (1969).
- [36] H. K. Armenian, G. R. Goldstein, J. P. Rutherford, and D. L. Weaver, Phys. Rev. **D12**, 1278 (1975).
- [37] P. D. B. Collins and T. D. B. Wilkie, Z. Phys. **C7**, 357 (1981).
- [38] <http://www.indiana.edu/~jpac/index.html>.
- [39] T. Trueman and G. Wick, Annals Phys. **26**, 322 (1964).
- [40] R. Childers and W. G. Hollady, Phys.Rev. **132**, 1809 (1963).
- [41] M. Jacob and G. Wick, Annals Phys. **7**, 404 (1959).
- [42] R. Workman, M. Paris, W. Briscoe, L. Tiator, S. Schumann, et al., Eur.Phys.J. **A47**, 143 (2011), 1102.4897.